

# Green's Function Brownian Dynamics: a new approach to simulate biochemical networks at the particle level and in time and space

Jeroen S. van Zon<sup>1,2</sup> and Pieter Rein ten Wolde<sup>1,2</sup>

<sup>1</sup>*FOM Institute for Atomic and Molecular Physics,  
Kruislaan 407, 1098 SJ Amsterdam, The Netherlands.*

<sup>2</sup>*Division of Physics and Astronomy, Vrije Universiteit,  
De Boelelaan 1081, 1081 HV Amsterdam, The Netherlands.*

(Dated: May 23, 2019)

Biochemical networks are the analog computers of life. They allow the living cell to control a large number of biological processes, such as gene expression and cell signalling. In the modeling of biochemical networks, it is standard practice to describe them by a set of macroscopic rate equations. In this approach, it is implicitly assumed that the concentrations of the molecules are large and that fluctuations can be neglected. In the living cell, however, molecules are often present in very low numbers. This means that the discrete nature of the reactants has to be taken into account. Moreover, the spatial distribution of the components can be of crucial importance. We have developed a new technique, called Green's Function Brownian Dynamics, that makes it possible to simulate biochemical networks at the particle level and in both time and space. Here, we apply it to a simple model of gene expression. The simulations reveal that the scheme is highly efficient. Under biologically relevant conditions, it can be up to five orders of magnitude faster than conventional particle-based techniques to simulate biochemical networks in time and space.

PACS numbers: 81.05.Rm, 05.20.Dd, 83.10.Pp

## I. INTRODUCTION

Most, if not all, organisms can be considered to be information processing machines. Even relatively simple organisms, such as the bacterium *Escherichia coli*, can perform fairly complex computations like: IF lactose is present AND NOT glucose is present, then use lactose. Recent technological developments have made it possible to acquire information on the regulatory architecture of the cell on an unprecedented scale. And extensive databases are now available that catalogue biochemical pathways. Yet, our understanding of the mechanisms that underlie the regulation of biochemical networks is still limited. One important reason is that biochemical networks are controlled by stochastic processes.

In the living cell, computations are performed by molecules that chemically and physically interact with each other. These components, that form what is called a biochemical network, behave stochastically. They move in an erratic fashion, namely by diffusion, and act upon each other in a stochastic manner - chemical reactions, and equally important, physical interactions are probabilistic in nature. These factors become particularly important when the concentrations are low. In the living cell, this is often the case, and, as a result, biochemical networks can be highly stochastic. In this respect, it is a remarkable fact that many biological processes operate reliably with surprisingly small numbers of molecules.

In order to understand how biochemical networks perform reliably in the presence of biochemical noise, the current numerical techniques are of limited use. Table I gives an overview of the different numerical techniques to analyse biochemical networks. The conventional approach is to write down the macroscopic rate equations

and to solve the corresponding differential equations numerically. In this approach, the evolution of the network is deterministic. It is implicitly assumed that the concentrations are large and that fluctuations can be neglected. A common approach to include the effect of fluctuations is to add a noise term to the macroscopic rate equations [1]. However, at low concentrations, this approach is bound to fail, as demonstrated by Togashi and Kaneko [2] and Shnerb and coworkers [3]. At low concentrations, we have to recognize the discrete nature of the reactants and the stochastic character of their interactions. Currently, two techniques exist to simulate biochemical networks at the particle level [4, 5, 6]. Both techniques are consistent with the chemical master equation. However, the chemical master equation relies on the assumption that there are many non-reactive collisions to stir the system between the reactive collisions. In effect, it treats the spatial fluctuations in a mean-field manner: at every instance, it is assumed that the particles are uniformly distributed in space. This is a serious limitation. First of all, spatial fluctuations can be a major source of noise in a biochemical network. Secondly, in the living cell, signals often have to be transmitted from one place to the next by the diffusive motion of "messenger" molecules; their concentrations can be non-uniform, and more importantly, their low mobility can limit the response time of the network. Moreover, many processes, such as the immune response, involve a complex spatial reorganisation of the reactants. And, finally, a large number of biological processes require the assembly of a complex of proteins, which can only be accurately described by a method that resolves the network in space.

Clearly, in many cases we have to describe the network at the particle level and in both time and space.

But, as discussed above, the current techniques cannot accomplish this. They either ignore the particulate nature of matter, or treat the spatial fluctuations in a mean-field manner. We have developed a new technique, called Green's Function Brownian Dynamics (GFBD), that makes it possible to simulate biochemical networks at the particle level and in time and space. In the next section, we describe the technique. In the subsequent section, we apply the technique to a simple model of gene expression. The calculations show that the technique is highly efficient; it is about five orders of magnitude faster than the brute-force approach. We thus believe that GFBD brings simulating biochemical networks at the particle level and in time and space within reach.

## II. NUMERICAL TECHNIQUE

### A. Introduction

In order to model biochemical networks at the particle level and in time and space, several approaches could be taken. Naturally, the choice of the method should be guided by the physics. Most proteins are believed to be transported by their diffusive motion, although in eucaryotic cells, cytoskeletal networks and motor proteins may facilitate the transport of molecules [7]. Such mechanisms of active transport have not been observed in bacteria. In bacteria, diffusion is the primary means of intracellular movement. Here, we will assume that the particles are transported by their diffusive motion, although the technique can be extended to include active transport as well.

Two approaches seem useful to simulate a biochemical network at the particle level and in time and space. The first is to let the particles undergo a random walk on a lattice and to let reaction partners react with a certain probability when they happen to meet each other. This technique is fast, but has a number of limitations, the most important of which are that the physical dimensions of the particles and the interactions between them cannot conveniently be described.

A more appealing technique is based upon Brownian Dynamics. Brownian Dynamics is a stochastic dynamics scheme, in which the particles are propagated according to the overdamped limit of the Langevin equation. In Brownian Dynamics, the solvent is considered implicitly; only the solute particles are considered explicitly. The forces experienced by these particles contain two parts: a conservative part, which arises from the interactions with the other solute particles, and a random part. The latter is the dynamical remnant of the solvent - the solutes are thought to experience random forces from the solvent. Via the fluctuation-dissipation theorem and the Einstein relation, the random forces are related to the diffusion constant of the particles. To be more explicit, the equations of motion for the solute particles are given

by:

$$\dot{\mathbf{r}}_s = \frac{D_s}{k_B T} (\mathbf{F}_s + \delta\mathbf{F}_s). \quad (1)$$

Here,  $\mathbf{r}_s$  denotes the position of solute particle  $s$ ,  $D_s$  is the diffusion constant of solute particle  $s$ ,  $k_B T$  is Boltzmann's constant times temperature,  $\mathbf{F}_s$  is the conservative force exerted by the other solute particles, and  $\delta\mathbf{F}_s$  is the random force that arises from the interactions with the solvent.

Brownian Dynamics has a number of advantages over lattice-based techniques: the particles move in continuum space; the interactions between particles - the potential of mean force - can easily be described; excluded volume effects are taken into account naturally; and to each type of particles a different diffusion constant can be assigned. Furthermore, the time step of the algorithm can be varied. This is of particular importance for biochemical networks, as the concentrations of the species can be very low. If the particles are far apart, then the motion of the particles is governed by unrestricted diffusion. For free diffusion, the probability  $p(\mathbf{r}, t | \mathbf{r}_0, t_0)$  that a particle will move from  $\mathbf{r}_0$  to  $\mathbf{r}$  in a time  $t - t_0$  is known analytically. Hence, the magnitude of the time step is only limited by the fact that at the end of the time step the particles interact with each other; the further the particles are apart, the larger the time step can be used. Finally, the propagation of the particles can elegantly be combined with the reactions between the particles.

To address this, it will be instructive to consider the reaction  $A + B \xrightarrow{k} C + D + \dots$ . In principle, this reaction can be straightforwardly implemented into the Brownian Dynamics scheme: the particles are propagated according to Eq. (1) and when two reaction partners happen to meet each other, they can react with a probability that is consistent with the rate constant  $k$ . The disadvantage of this scheme, however, is that very small time steps are needed in order to resolve the collision events.

The reaction events can be more efficiently incorporated into the Brownian Dynamics scheme. To see this, one should realize that Brownian Dynamics is, in effect, a *numerical* procedure for solving the Smoluchowski equation. For a pair of particles, that not only move diffusively, but also can react according to  $A + B \xrightarrow{k} C + D + \dots$ , the Smoluchowski equation can be solved *analytically* using Green's functions. The main idea of GFBD is to exploit the exact solution for a pair of particles to set up an event-driven algorithm. This allows GFBD to make large jumps in time when the particles are far apart from each other. In biochemical networks this is often the case as the reactant concentrations are usually low. GFBD is therefore ideally suited for biochemical networks. Below we describe the scheme in more detail.

Description		Accounts for spatial extent of network	Incorporates fluctuations
Digital	Boolean	No	No
Continuum	Ordinary differential equations	No	No
	Stochastic differential equations	No	Only at high concentrations
	Reaction diffusion equations	Yes	No
Particle-based	Chemical master equation	No	Yes
	GFBD	Yes	Yes

TABLE I: Overview of existing techniques and the developed technique, called Green’s Function Brownian Dynamics (GFBD), to simulate biochemical networks. GFBD takes both the discrete nature and the spatial distribution of the reactants into account.

### B. Overview of the algorithm

Let us imagine a configuration of reactants as shown in Fig. 1. The circles indicate the distances the particles can travel in a time step  $\Delta t$ . For a particle that moves by free diffusion with a diffusion constant  $D$ , that distance scales as  $\langle \Delta \mathbf{r}^2(\Delta t) \rangle \sim D\Delta t$ . Clearly, the larger the time step, the larger the probability that reaction partners meet and react with each other. However, we cannot make the time

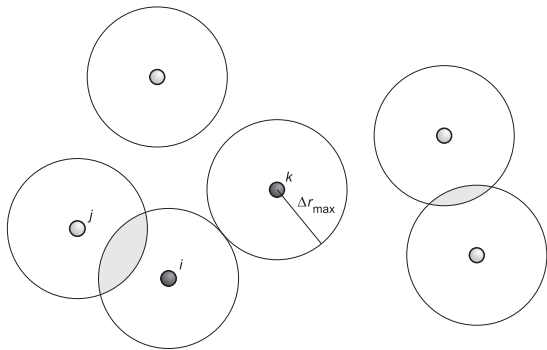


FIG. 1: Determination of the maximum time step,  $\Delta t_{\max}$ . The maximum size of the time step is set by the requirement that each particle can interact with at most one other particle during that time step. This means that each particle  $i$  can travel a distance of at most  $\Delta r_{\max,i}$ . We have used the operational criterion  $\Delta r_{\max,i} = H\sqrt{6D_i\Delta t_{\max,i}}$ , with  $D_i$  being the diffusion constant of particle  $i$ . A value of  $H = 3$  was found to yield a good conservation of the correct steady-state distribution. In this example, each particle is assumed to have the same diffusion constant; the time step is limited by the constraint that particles  $i$  and  $k$  should not interact as particle  $i$  can already interact with particle  $j$ . Note that with this maximum time step the many-body problem of propagating the  $N$  particles is reduced to that of propagating single particles and pairs of particles.

step arbitrarily large: if a given particle can collide with more than one other particle during a time step, then the problem becomes a many-body problem that we can not solve analytically. The size of a time step is thus limited by the requirement that each particle can interact with at most one other particle during that time step. This constraint sets an upper limit on the magnitude of a time step in our algorithm; we will call it  $\Delta t_{\max}$ . However, provided that we consider times  $\Delta t$  smaller than  $\Delta t_{\max}$ , the problem can now be reduced to that of propagating single particles and pairs of particles. This problem can be solved analytically using Green’s functions, as we will describe now.

### C. Monomolecular reactions - the Green’s function for single particles

In this section, we consider the propagation of a *single* particle. We assume that the particle is spherical in shape and moves by free diffusion with a diffusion constant  $D$ . The diffusive motion of the particle is described by the Einstein diffusion equation

$$\partial_t p(\mathbf{r}, t | \mathbf{r}_0, t_0) = D\nabla^2 p(\mathbf{r}, t | \mathbf{r}_0, t_0). \quad (2)$$

Here,  $p(\mathbf{r}, t | \mathbf{r}_0, t_0)$  is the probability that the particle is at position  $\mathbf{r}$  at time  $t$ , given that it was at  $\mathbf{r}_0$  at time  $t_0$ . This diffusion equation can be solved subject to the initial condition and the boundary condition

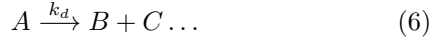
$$p(\mathbf{r}, t_0 | \mathbf{r}_0, t_0) = \delta(\mathbf{r} - \mathbf{r}_0), \quad (3)$$

$$p(|\mathbf{r}| \rightarrow \infty, t | \mathbf{r}_0, t_0) = 0, \quad (4)$$

respectively. The solution  $p(\mathbf{r}, t | \mathbf{r}_0, t_0)$  is known as Green’s function. It is given by the well-known expression

$$p(\mathbf{r}, t | \mathbf{r}_0, t_0) = \frac{1}{[4\pi D(t - t_0)]^{3/2}} \exp\left[-\frac{(\mathbf{r} - \mathbf{r}_0)^2}{4D(t - t_0)}\right]. \quad (5)$$

It is conceivable that the particle does not only move diffusively, but also can “decay” according to



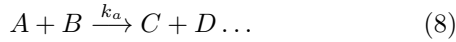
We will assume that, if the reaction happens, it happens *instantaneously*. This means that the reaction can be decoupled from the diffusive motion of the particle. If  $k_d dt$  is the probability that a reaction occurs in an infinitesimal time interval  $dt$ , then the probability that the *next* reaction occurs between  $t$  and  $t + dt$ , is

$$q_d(t|t_0)dt = k_d \exp[-k_d(t - t_0)] dt. \quad (7)$$

In section II E, we will use Eqs. 5 and 7 to set up an event-driven algorithm.

#### D. Bimolecular reactions - the Green’s function for pairs of particles

In this section, we consider *one pair* of particles  $A$  and  $B$  that can react according to



We again assume that the particles  $A$  and  $B$  are spherical in shape and move by their diffusive motion; the diffusion constants for particle  $A$  and  $B$  are  $D_A$  and  $D_B$ , respectively. Furthermore, we assume that the particles react with an intrinsic rate constant  $k_a$  when they have approached each other within the reaction distance  $\sigma = (d_A + d_B)/2$ , where  $d_A$  and  $d_B$  are the diameters of particles  $A$  and  $B$ , respectively. In addition, we imagine that the particles interact with each other via a potential  $U(\mathbf{r})$ , where  $\mathbf{r} = \mathbf{r}_B - \mathbf{r}_A$ . The force acting on particle  $B$  is thus given by  $-\nabla_B U(\mathbf{r}) = \mathbf{F}(\mathbf{r})$ , while the force acting on particle  $A$  is given by  $-\mathbf{F}(\mathbf{r})$ .

We aim to derive the distribution function  $p(\mathbf{r}_A, \mathbf{r}_B, t | \mathbf{r}_{A0}, \mathbf{r}_{B0}, t_0)$ , which yields the probability that the particles  $A$  and  $B$  are at positions  $\mathbf{r}_A$  and  $\mathbf{r}_B$  at time  $t$ , given that they are at  $\mathbf{r}_{A0}$  and  $\mathbf{r}_{B0}$  at time  $t_0$ . This distribution function satisfies for  $|\mathbf{r}| \geq \sigma$  the following Smoluchowski equation

$$\begin{aligned} \partial_t p(\mathbf{r}_A, \mathbf{r}_B, t | \mathbf{r}_{A0}, \mathbf{r}_{B0}, t_0) = & \\ [D_A \nabla_A^2 + D_B \nabla_B^2 - D_B \beta \nabla_B \cdot \mathbf{F}(\mathbf{r}) + D_A \beta \nabla_A \cdot \mathbf{F}(\mathbf{r})] & \\ \times p(\mathbf{r}_A, \mathbf{r}_B, t | \mathbf{r}_{A0}, \mathbf{r}_{B0}, t_0). & \end{aligned} \quad (9)$$

It will be convenient to make a coordinate transformation

$$\mathbf{R} = \sqrt{D_B/D_A} \mathbf{r}_A + \sqrt{D_A/D_B} \mathbf{r}_B, \quad (10)$$

$$\mathbf{r} = \mathbf{r}_B - \mathbf{r}_A, \quad (11)$$

and to define the operators

$$\nabla_{\mathbf{R}} = \partial/\partial \mathbf{R}, \quad (12)$$

$$\nabla_{\mathbf{r}} = \partial/\partial \mathbf{r}. \quad (13)$$

Eq. 9 can then be rewritten as:

$$\begin{aligned} \partial_t p(\mathbf{R}, \mathbf{r}, t | \mathbf{R}_0, \mathbf{r}_0, t_0) = & (D_A + D_B) [\nabla_{\mathbf{R}}^2 + \nabla_{\mathbf{r}} \cdot (\nabla_{\mathbf{r}} - \mathbf{F}(\mathbf{r}))] \\ & \times p(\mathbf{r}_A, \mathbf{r}_B, t | \mathbf{r}_{A0}, \mathbf{r}_{B0}, t_0), \\ & |\mathbf{r}| \geq \sigma. \end{aligned} \quad (14)$$

It is seen that Eq. 14 describes two independent random processes - free diffusion in the coordinate  $\mathbf{R}$  and diffusion with a drift in the coordinate  $\mathbf{r}$ . This means that the distribution function  $p(\mathbf{r}_A, \mathbf{r}_B, t | \mathbf{r}_{A0}, \mathbf{r}_{B0}, t_0)$  can be factorized as  $p(\mathbf{R}, t | \mathbf{R}_0, t_0) p(\mathbf{r}, t | \mathbf{r}_0, t_0)$  and that the above equation can be reduced to one Smoluchowski equation for the coordinate  $\mathbf{R}$  and one for the coordinate  $\mathbf{r}$ :

$$\begin{aligned} \partial_t p(\mathbf{R}, t | \mathbf{R}_0, t_0) = & (D_A + D_B) \nabla_{\mathbf{R}}^2 \\ & \times p(\mathbf{R}, t | \mathbf{R}_0, t_0), \end{aligned} \quad (15)$$

$$\begin{aligned} \partial_t p(\mathbf{r}, t | \mathbf{r}_0, t_0) = & (D_A + D_B) \nabla_{\mathbf{r}} \cdot (\nabla_{\mathbf{r}} - \mathbf{F}(\mathbf{r})) \\ & \times p(\mathbf{r}, t | \mathbf{r}_0, t_0), \quad |\mathbf{r}| \geq \sigma. \end{aligned} \quad (16)$$

Eqn. 15 describes the free diffusive motion of the coordinate  $\mathbf{R}$ . The solution of that equation, for the initial condition  $p(\mathbf{R}, t_0 | \mathbf{R}_0, t_0) = \delta(\mathbf{R} - \mathbf{R}_0)$  and boundary condition  $p(|\mathbf{R}| \rightarrow \infty, t | \mathbf{R}_0, t_0) = 0$ , is

$$p(\mathbf{R}, t | \mathbf{R}_0, t_0) = \frac{\exp\left[-\frac{(\mathbf{R} - \mathbf{R}_0)^2}{4(D_A + D_B)(t - t_0)}\right]}{[4\pi(D_A + D_B)(t - t_0)]^{3/2}}. \quad (17)$$

The non-trivial solution is that of the Smoluchowski equation for the interparticle vector  $\mathbf{r}$ . This solution also has to take into account the reactions between  $A$  and  $B$ . We will incorporate the reaction as a boundary condition on the solution of the Smoluchowski equation. To be more explicit, the initial condition and boundary conditions for the coordinate  $\mathbf{r}$  are given by

$$p(\mathbf{r}, t_0 | \mathbf{r}_0, t_0) = \delta(\mathbf{r} - \mathbf{r}_0), \quad (18)$$

$$p(|\mathbf{r}| \rightarrow \infty, t | \mathbf{r}_0, t_0) = 0, \quad (19)$$

$$\begin{aligned} -j(\sigma, t | \mathbf{r}_0, t_0) \equiv & 4\pi\sigma^2 D \left( \frac{\partial}{\partial r} - \mathbf{F}(\mathbf{r}) \right) \\ & \times p(\mathbf{r}, t | \mathbf{r}_0, t_0) \Big|_{|\mathbf{r}|=\sigma}, \\ = & k_a p(|\mathbf{r}| = \sigma, t | \mathbf{r}_0, t_0), \end{aligned} \quad (20)$$

where  $\partial/\partial r$  denotes a derivative with respect to the interparticle separation  $r$ . It is seen that the reaction enters the problem as a third boundary condition on the solution of the Smoluchowski equation. Here  $j(\sigma, t | \mathbf{r}_0, t_0)$  is the outward radial flux of probability  $p(\mathbf{r}, t | \mathbf{r}_0, t_0)$  through the “contact” surface of area  $4\pi\sigma^2$ . The boundary condition, also known as a *radiation* boundary condition [9, 10], states that this radial flux of probability equals the intrinsic rate constant times the probability that the particles  $A$  and  $B$  are, in fact, in contact. In the limit  $k_a \rightarrow \infty$ , the radiation boundary condition reduces to an *absorbing* boundary condition  $p(|\mathbf{r}| = \sigma, t | \mathbf{r}_0, t_0) = 0$ , while in the limit  $k_a \rightarrow 0$  the radiation boundary condition reduces to a *reflecting* boundary condition.

The Green's function  $p(\mathbf{r}, t|\mathbf{r}_0, t_0)$  is derived in the appendix. Here, we will discuss some useful quantities that can be derived from the Green's function. The first quantity of interest is the probability that a pair of particles, initially separated by  $\mathbf{r}_0$ , survives and does not recombine by time  $t$ . This so-called *survival* probability is given by

$$S_a(t|\mathbf{r}_0, t_0) = \int_{|\mathbf{r}|>\sigma} d\mathbf{r} p(\mathbf{r}, t|\mathbf{r}_0, t_0). \quad (21)$$

Clearly,  $S_a(0|\mathbf{r}_0, t_0) = 1$  for  $|\mathbf{r}_0| > \sigma$ . The second quantity of interest is the reaction rate  $q_a(t|\mathbf{r}_0, t_0)$ , which is defined as the probability per unit time that a pair, initially separated by  $\mathbf{r}_0$ , reacts at time  $t$ . It is related to the survival probability by

$$q_a(t|\mathbf{r}_0, t_0) \equiv -\frac{\partial S_a(t|\mathbf{r}_0, t_0)}{\partial t}. \quad (22)$$

Since the reactions are assumed to occur only at contact, the reaction rate is also given by the flux at contact

$$q_a(t|\mathbf{r}_0, t_0) = -j(\sigma, t|\mathbf{r}_0, t_0). \quad (23)$$

The above equation can also be obtained from Eq. 16 and Eq. 21 and by using the fact that the flux at  $|\mathbf{r}| \rightarrow \infty$  vanishes.

The reaction rate  $q_a(t|\mathbf{r}_0, t_0)$  can be interpreted as the probability that the *next* reaction for a pair of particles, initially separated by  $\mathbf{r}_0$ , occurs at time  $t$ . As such, it can be used to set up an event-driven algorithm, which we will describe in the next section.

### E. Outline of the algorithm

To explain the essence of the algorithm, it will be instructive to consider a single particle  $A$  that can react with a single particle  $B$  according to the following scheme



Furthermore, it will be useful to imagine that neighbouring particles limit the size of the time step to  $\Delta t_{\max}$ . The event-driven algorithm would then consist of iterating the following steps: 1) if particles  $A$  and  $B$  are not bound to each other, then draw a next association time  $t$  according to  $q_a(t|\mathbf{r}_0, t_0)$  (Eq. 22). a) If  $(t - t_0) \geq \Delta t_{\max}$ , then the two particles will not react within the time step; new positions for  $A$  and  $B$  at time  $t_0 + \Delta t_{\max}$  are obtained from  $p(\mathbf{R}, t_0 + \Delta t_{\max}|\mathbf{R}_0, t_0)$  (Eq. 17) and  $p(\mathbf{r}, t_0 + \Delta t_{\max}|\mathbf{r}_0, t_0)$  (Eq. 40). b) if  $(t - t_0) < \Delta t_{\max}$ , then the next reaction will occur within the time step; a new position for particle  $C$  at time  $t$  is obtained from  $p(\mathbf{R}, t|\mathbf{R}_0, t_0)$  (Eq. 17). 2) if particles  $A$  and  $B$  are bound and form the particle  $C$ , then draw a next dissociation time from  $q_d(t|\mathbf{r}_0, t_0)$  (Eq. 7). a) If  $(t - t_0) \geq \Delta t_{\max}$ , then particle  $C$  has not decayed at  $t_0 + \Delta t_{\max}$ ; a new position for  $C$  at time  $t_0 + \Delta t_{\max}$  is obtained from  $p(\mathbf{r}, t_0 + \Delta t_{\max}|\mathbf{r}_0, t_0)$  (Eq. 5);

b) if  $(t - t_0) < \Delta t_{\max}$ , the next reaction has occurred within the maximum time step; the particles  $A$  and  $B$  are placed at time  $t$  at positions centered around  $\mathbf{r}$  as obtained from  $p(\mathbf{r}, t|\mathbf{r}_0, t_0)$  (see Eq. 5).

The procedure outlined above forms the heart of the algorithm. The crux of the method is to choose the maximum time step such that only monomolecular reactions or bimolecular reactions have to be considered. This makes it possible to use the exact solution of the Smoluchowski equation to propagate the system to the next reaction event in a single step. The full algorithm for a system of  $N$  particles thus consists of iterating the following steps:

1. Determine maximum time step  $\Delta t_{\max}$ . The maximum time step is determined by the condition that only single particles or pairs of particles have to be considered (see section II B and Fig. 1). For each particle  $i$ , we determine the maximum time step  $\Delta t_{\max, i}$ , such that it can interact with at most one other particle. The maximum global time step is then given by

$$\Delta t_{\max} = \min(\{\Delta t_{\max, i}\}). \quad (25)$$

In order to determine  $\Delta t_{\max, i}$  for particle  $i$ , we assume that during that step the particle can travel at most a distance  $\Delta r_{\max, i} = H\sqrt{6D_i\Delta t}$ , where  $D_i$  is the diffusion constant of particle  $i$ . We found that  $H = 3$  suffices to preserve the correct steady-state distribution.

2. Determine next reaction and next reaction time.

We first construct a list of possible reactions  $\{R_\nu\}$ . With each reaction  $R_\nu$ , we associate a survival probability function  $S_\nu(t - t_0)$  and a next-reaction distribution function  $q_\nu(t - t_0)$ ; the two are related via  $q_\nu(t - t_0) = -\partial S_\nu(t - t_0)/\partial t$ . For the bimolecular reactions,  $q_\nu(t - t_0) = q_a(t|\mathbf{r}_0, t_0)$  as given by Eq. 22 and  $S_\nu(t - t_0) = S_a(t|\mathbf{r}_0, t_0)$  as given by Eq. 21. For the monomolecular reactions,  $q_\nu(t - t_0) = q_d(t|t_0) = k_d \exp(-k_d(t - t_0))$  and  $S_\nu(t - t_0) = \exp(-k_d(t - t_0))$ .

For each reaction  $R_\nu$ , we generate a random number  $\xi_\nu$ , uniformly distributed in the interval  $0 < \xi_\nu < 1$ . If  $\xi_\nu \leq (1 - S_\nu(\infty))$ , a tentative next reaction time  $\Delta t_\nu$  is obtained from

$$\xi_\nu = \int_0^{\Delta t_\nu} q_\nu(t') dt' = 1 - S_\nu(\Delta t_\nu). \quad (26)$$

If, however,  $\xi_\nu > (1 - S_\nu(\infty))$ , then the reaction  $R_\nu$  does not occur and it is dropped from the list of possible reactions. From the remaining list of tentative reactions, we choose as the actual next reaction the one that occurs first, *provided* that this reaction occurs within the maximum time step  $\Delta t_{\max}$ . Concomittantly, the system is propagated through a time  $\Delta t$  as given by

$$\Delta t = \min(\{\Delta t_\nu\}, \Delta t_{\max}). \quad (27)$$

Note that if there is no tentative reaction for which the tentative next reaction time  $\Delta t_\nu < \Delta t_{\max}$ , then no reaction will occur within the time step. Here, we also mention for completeness that for association reactions  $S_\nu(\infty) \neq 0$ : for two particles, that can diffuse and react subject to the boundary condition Eq. 19, there is a finite probability that they *never* react; this is related to the well-known fact that a random walker, who starts at the origin, can “escape” and never return to the origin.

3. Propagate particles. The single particles are propagated according to  $p(\mathbf{r}, t | \mathbf{r}_0, t_0)$  in Eq. 5. For each pair of particles, the following two substeps are executed: 1) a new position for the coordinate  $\mathbf{R}$  is obtained from Eq. 17; 2) if the pair has not reacted, a new interparticle vector  $\mathbf{r}$  is obtained from  $p(\mathbf{r}, t | \mathbf{r}_0, t_0)$  in Eq. 40; else, if it has reacted, the products are placed at positions around  $|\mathbf{r}| = 0$ .
4. Update particles. Update identities of particles according to the executed reaction. Delete or add particles created or destroyed in reaction.

A proof of the algorithm is given in appendix B.

### III. RESULTS

This section is organized as follows: first we study a simple bimolecular reaction to show that GFBD accurately reproduces theoretical results. Then we turn our attention to two very simple models of gene expression as typical examples of systems that are well handled by the GFBD technique. We specifically focus on the levels of noise in protein concentrations and find dramatic differences between GFBD and results from the chemical master equation, that ignores spatial fluctuations. Finally we compare the performance of GFBD to a conventional Brownian Dynamics algorithm.

#### A. Bimolecular reaction

To test the validity of our approach, we study the reversible bimolecular reaction



with forward rate constant  $k_a$  and backward rate constant  $k_d$ . As a first test of our algorithm, we calculate  $p(r, t | r_0, t_0)$  for an *isolated* pair of particles and compare the numerical result to the analytical result for the spherically symmetric Green’s function as recently derived by Kim and Shin [8]. In order to compute  $p(r, t | r_0, t_0)$ , we use a set up in which particle  $A$  is placed at the origin and held fixed during the simulation. A second particle  $B$  is initially placed at random in a spherical shell of

radius  $r_0$  centered around particle  $A$ . We then propagate particle  $B$  for a time  $t_{\text{sim}}$ . During this time, particle  $B$  can diffuse freely with a diffusion constant  $D$  and it can associate with particle  $A$  with a rate constant  $k_a$  and dissociate from it with a rate constant  $k_d$ . Typically, particle  $B$  will associate with and dissociate from  $A$  a (large) number of times during the simulation. We repeat this procedure many times, which allows us to calculate  $p(r, t | r_0, t_0)$ .

If the next reaction time would be larger than the simulation time,  $t_{\text{sim}}$ , then we could in principle directly propagate the particles through  $t_{\text{sim}}$ . However, this would not provide a stringent test of our algorithm. At each step, we therefore choose a maximum time step  $\Delta t_{\max}$  at random from the interval  $[0.05, t_{\text{sim}}]$ . This could be interpreted as mimicking the constraint on the maximum time step arising from the presence of other particles.

Figure 2 shows excellent agreement for  $p(r, t | r_0)$  between theory and simulation. We find similar agreement between theory and simulation for other initial distances  $r_0$  and for other values of the diffusion constant  $D$  and reaction rates  $k_a$  and  $k_d$ . It should be realized that because the particles are initially placed at contact, many reactions can occur during the time  $t_{\text{sim}}$ . Moreover, because we divide the simulation time in smaller intervals, we must propagate the particles many times, using the Green’s function for an extensive range of parameters. Thus, at least for the case of an isolated pair of particles, this procedure provides a thorough test of our algorithm.

Next, we want to study a more complex system in

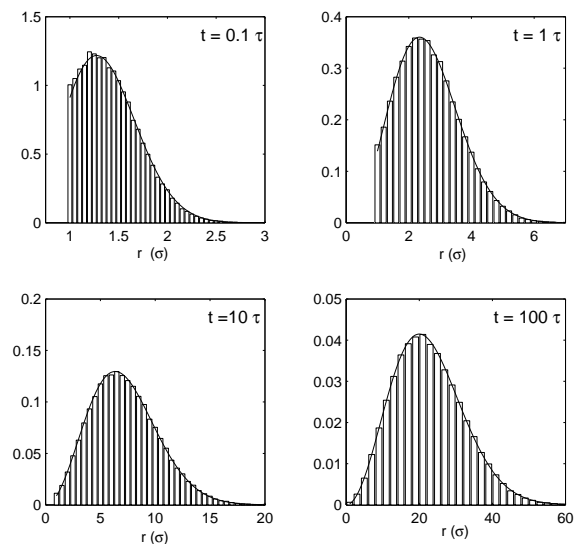


FIG. 2: The distribution  $p(r, t | \sigma, t_0 = 0)$  for  $t = 0.1\tau$ ,  $1\tau$ ,  $10\tau$  and  $100\tau$ . For  $r < \sigma$ , the distribution  $p(r, t | \sigma, t_0) = 0$  due to the hard sphere repulsion between the particles. The bars denote the simulation results and the solid lines denotes the analytical solutions of Kim and Shin [8]. Note that the particles are initially placed at contact ( $r_0 = \sigma$ ). The forward rate constant  $k_a = 4.65 \text{ molecule}^{-1} \sigma^3 \tau^{-1}$  and the backward rate constant is  $k_d = 1 \tau^{-1}$ . The unit of time  $\tau = \sigma^2/D$ .

which a single particle  $A$  is held fixed at the center of a spherical container of radius  $R$  and is surrounded by  $N_B$  particles  $B$ . Particles  $A$  and  $B$  can again react according to the scheme in Eq. 28. Particles  $B$  and  $C$  cannot react, although they also should not overlap with each other. The excluded volume interactions between a pair of two  $B$  particles and a pair of a  $B$  and a  $C$  particle is taken into account by using reflecting boundary conditions, i.e. by setting  $k_a = 0$  in Eq. 20. We note that the requirement that the  $B$  and  $C$  particles are not allowed to overlap, imposes a constraint on the maximum size of the time step,  $\Delta t_{\max}$ . The wall of the container is assumed to be reflecting. As no analytical solution exists for a *pair* of particles in the presence of a reflecting boundary, we introduce the further requirement that during a time step a particle can only interact with either the wall of the container or with another particle, but not with both.

As the  $B$  particles diffuse through the container, they will come into contact with the fixed particle  $A$ . When in contact, the particles  $A$  and  $B$  can enter the *bound* state  $C$  with forward rate  $k_a$ . When in the bound state, other  $B$  particles approaching the fixed  $C$  particle cannot react with it. Only after dissociation into the unbound state  $A + B$ , occurring at rate  $k_d$ , another reaction can occur. On average, there will be a probability  $p_{\text{bound}}$  of finding the  $A$  particle bound to the  $B$  particle. It is given by

$$p_{\text{bound}} = \frac{g_{AB}(\sigma)KN_B}{V + g_{AB}(\sigma)KN_B}, \quad (29)$$

where  $K = k_a/k_d$  is the equilibrium constant,  $V = 4/3\pi[(R - \sigma/2)^3 - \sigma^3]$  is the volume available for the  $B$  particles and  $N_B$  is the *total* number of  $B$  particles. The function  $g_{AB}(r)$  is the radial distribution function for the pair of particles  $A$  and  $B$ .

The radial distribution function  $g_{AB}(r)$  describes the spatial correlations arising from the interactions between the particles [11]. It is conceivable that in this system the excluded volume interactions between the particles induce spatial correlations. These correlations could affect the density of  $B$  particles that are in contact with the  $A$  particle and thereby the probability that the  $A$  particle is bound to a  $B$  particle. In Eq. 29, the distribution function at contact,  $g_{AB}(\sigma)$ , thus describes the effect of the spatial correlations on the average occupancy of the  $A$  particle. However, the concentrations that we consider here are very low and, as a result, the spatial correlations are very small. Indeed, the simulations reveal that  $g_{AB}(r) \approx 1$  for all distances  $r$ . If  $g_{AB}(\sigma) = 1$ , then Eq. 29 reduces to the well-known mean-field result that can straightforwardly be obtained from the macroscopic rate equations. In Fig. 3, we compare the simulation results to the mean-field prediction. We find excellent agreement.

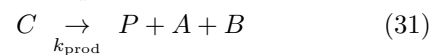
In conclusion, we have shown that our algorithm provides an accurate way of simulating an assembly of particles that can move by diffusion and react according to monomolecular and bimolecular reactions. As more complicated reactions, such as trimolecular reactions, can, in

general, be decomposed into these elementary reactions, we are now in a position to simulate more complex systems.

## B. Gene expression I

In this section we present results for a model of gene expression. It should be stressed that the model is highly simplified. The purpose here is to show the power of our approach. Yet, we find interesting effects due to the spatial fluctuations of the components that could be of relevance for more realistic systems.

The reaction network consists of the following reactions:



In this picture,  $A$  is a promoter region on the DNA and  $B$  a RNA polymerase molecule that moves by free diffusion and can bind with a forward rate  $k_a$  to the promoter site to form the RNAP-DNA complex  $C$ . This complex can dissociate with a rate constant  $k_d$ . On the other hand, it can also produce a protein  $P$  at a production rate  $k_{\text{prod}}$ . Proteins degrade with a decay rate  $k_{\text{dec}}$ . Note that when a protein is produced the RNAP dissociates from the DNA.

In the living cell, the concentration of free RNAP – RNAP that is not bound to the DNA – is usually very

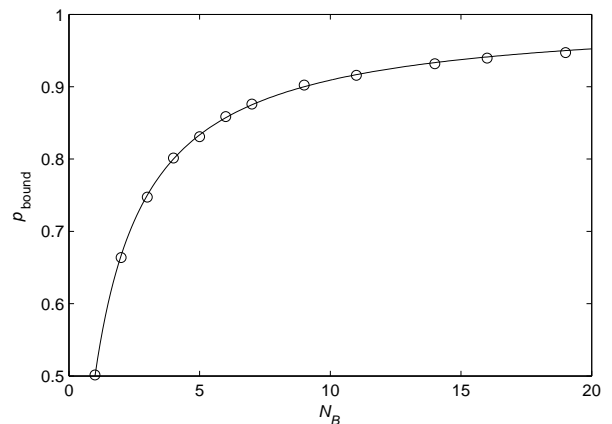


FIG. 3: The probability  $p_{\text{bound}}$  that the  $A$  particle is bound to a  $B$  particle as a function of the total number of  $B$  particles for the reaction scheme shown in Eq. 28. The symbols indicate the simulation results, while the dashed line denotes the mean-field prediction (Eq. 29 with  $g_{AB}(\sigma) = 1$ ). The radius of the container is  $R = 200\sigma$  and the equilibrium constant is chosen such that it is equal to the interaction volume  $V$ . The error bars in the simulation results are smaller than the size of the symbols.

low [13]. As a result, spatial correlations are negligible and the mean number of proteins,  $\overline{N}_P$ , can be obtained from the macroscopic rate equations. The result is:

$$\overline{N}_P = K_1 K_2 \frac{N_B}{V + K_1 N_B}. \quad (33)$$

Here  $K_1 = k_a/(k_d + k_{\text{prod}})$  and  $K_2 = k_{\text{prod}}/k_{\text{dec}}$  and  $N_B$  is again the total number of  $B$  molecules.

In the simulations, we fix the promoter site, i.e. the  $A$  particle, in the center of a spherical container of radius  $R$ . The volume of the container is  $V = 1\mu\text{m}^3$ , which is comparable to the volume of the cell of *Escherichia coli*. The promoter site is surrounded by  $N_B = 18$  RNAP molecules, corresponding to the concentration of free RNAP of 30 nM as found in the living cell [13]. The RNAP molecules move with a diffusion constant  $D = 1\mu\text{m}^2\text{s}^{-1}$ , which is comparable to that of similarly sized proteins as measured in [12]. We assume that, at contact, the RNAP can associate with the promoter site with a rate as determined by the Maxwell-Boltzmann velocity distribution. This leads to  $k_a = \pi\sigma^2\langle v_{AB} \rangle = 3 \cdot 10^9\text{M}^{-1}\text{s}^{-1}$ , where  $v_{AB}$  is the relative velocity of the particles  $A$  and  $B$ . We note that this estimate is equal to the rate of collisions between hard spheres in the low density limit [11, 14]. We could arrive at an alternative estimate for  $k_a$  using the diffusion constant and a molecular ‘‘jump’’ distance  $\lambda$ . This would lead to  $k_a = 4\pi\sigma^2 D/\lambda$ . Both estimates give similar results for the value of  $k_a$ . The dissociation rate is chosen such that the equilibrium constant  $K = k_a/k_d$  equals the one reported in [13], yielding  $k_d = 21.5\text{s}^{-1}$ . We assume that the diameters of the promoter site and the RNAP molecules are equal and given by  $\sigma = 5\text{nm}$ .

Here, we only simulate the promoter site and the RNAP molecules explicitly in space. The proteins are assumed to be uniformly distributed in space. Moreover, we assume that the proteins are both produced and degraded in a single step via a Poisson process. These assumptions are unrealistic, but they do demonstrate the power and the flexibility of our approach. In particular, the production and decay reactions can simply be added to our list of possible reactions,  $\{R_\nu\}$  (see section II E). The next-reaction distribution function for the production reaction is given by  $q_{\text{prod}}(t) = k_{\text{prod}} N_C \exp(-k_{\text{prod}} N_C t)$ , where  $N_C = 0$  if the RNAP is unbound and  $N_C = 1$  if it is bound to the DNA, while the propensity function for the degradation reaction is given by  $q_{\text{decay}}(t) = k_{\text{decay}} N_P \exp(-k_{\text{decay}} N_P t)$ . Hence, the GFBD scheme to simulate biochemical networks at the particle level and in time and space, can naturally be combined with kinetic Monte Carlo schemes that are based upon the chemical master equation, such as the Gillespie algorithm [4, 5].

In figure 4 we show the mean number of proteins  $\overline{N}_P$  as a function of the protein production rate  $k_{\text{prod}}$ , while keeping the decay rate fixed at  $k_{\text{decay}} = 0.04\text{s}^{-1}$ . As the concentration of the RNAP is low and spatial correlations are expected to be negligible, the simulation results for

the *average* number of proteins,  $\overline{N}_P$ , should follow the mean-field prediction of Eq. 33. Fig. 4 shows that this is indeed the case. However, in contrast to the mean-field analysis, the GFBD simulations allow us to quantify the effect of the *spatial fluctuations* of the RNAP molecules on the *noise* in the protein synthesis.

We can quantify the magnitude of the noise in protein production by computing the following quantity [13]:

$$\eta_P^2 = \frac{\overline{N_P^2(t)} - \overline{N}_P^2}{\overline{N}_P^2}. \quad (34)$$

Fig. 5 shows the result. Here we show the noise in the protein concentration as a function of the synthesis rate. In this analysis we have changed the degradation rate such that the average number of proteins,  $\overline{N}_P$ , is constant. The reason is that we want to focus on the effect of spatial fluctuations on the noise in protein production – we thus want to eliminate the fairly trivial changes in the noise due to changes in the average number of proteins.

Since we are interested in the importance of spatial fluctuations in gene expression, it is natural to compare the GFBD results to those obtained using the chemical master equation. The latter approach does take into account the discrete nature of the reactants and the stochastic character of their interactions, but it treats the spatial fluctuations in a mean-field manner: at each instance, it is implicitly assumed that the particles are uniformly distributed in space. This approach is justified if there are many non-reactive collisions to stir the system in between the reactive collisions. However, the RNAP is present in low copy numbers, and, upon contact, it rapidly associates with the promoter site on the DNA. As a consequence, this reaction is diffusion-limited. This could have importance implications for the noise in gene expression.

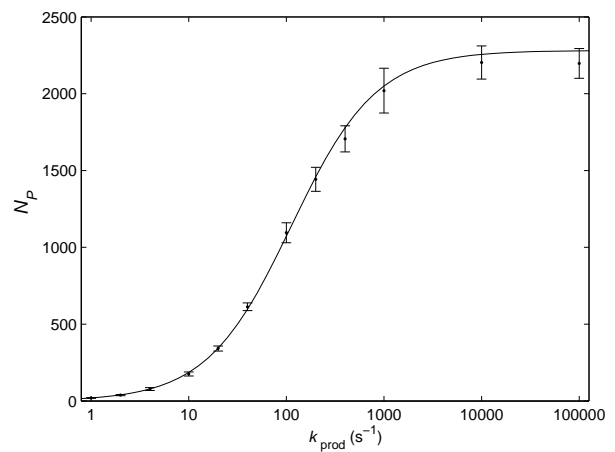


FIG. 4: The mean protein number  $\overline{N}_P$  as a function of the protein production rate  $k_{\text{prod}}$  as obtained from the GFBD simulations for the reaction scheme shown in Eqs. 30 – 32. The solid line denotes the mean-field prediction given by Eq. 33.



Using the techniques described in [1], we can analytically obtain the noise from the chemical master equation. It is given by

$$\eta_P^2 = \frac{1}{\bar{N}_P} - \frac{k_{\text{prod}}k_a N_B}{k_{\text{prod}}k_a N_B + \bar{N}_P(k_a N_B + k_d + k_{\text{prod}})^2}. \quad (35)$$

The first term on the right describes the result that would have been obtained if gene expression were a simple linear birth-and-death process. The second term reflects the fact that in order to produce a protein, it is necessary, albeit not sufficient, for a RNAP molecule to bind to the promoter site. This term, and thus the noise in gene expression, goes through a minimum at  $k_{\text{prod}} = k_a N_B + k_d$  and vanishes for both small and large  $k_{\text{prod}}$ . In these regimes, gene expression reduces to a simple linear birth-and-death process. In the limit of small  $k_{\text{prod}}$ , the production of the protein is the rate limiting step. The RNAP molecule will associate to and dissociate from the promoter site a large number of times, before it actually induces gene expression. The former process is thus in equilibrium on the time scale of gene expression. Hence, the birth term is given by  $k_{\text{birth}} = p_{\text{bound}}k_{\text{prod}}$ , with  $p_{\text{bound}}$  being the probability that a RNAP molecule is bound to the promoter (see Eq. 29); the death term is given by  $k_{\text{death}} = k_{\text{decay}}$ . In the limit of large  $k_{\text{prod}}$ , the binding of a RNAP molecule to the promoter site is the rate limiting step: as soon as a RNAP molecule is bound to the promoter, a protein will be produced. This means that the birth term is given by  $k_{\text{birth}} = k_a(1 - p_{\text{bound}})[\text{RNAP}]$ ; the death term is again  $k_{\text{death}} = k_{\text{decay}}$ . For a linear birth-and-death process, the noise is determined by the average number of proteins,  $\eta_P = 1/\sqrt{\bar{N}_P}$  [1]. As we have set the decay rate  $k_{\text{decay}}$  such that  $\bar{N}_P$  is constant, the noise in gene expression must be the same in the limiting regimes of small and large  $k_{\text{prod}}$ , in which gene expression reduces to a birth-and-death process.

Fig. 5 shows the comparison of the GFBD results to those obtained using the chemical master equation. It is seen that for small  $k_{\text{prod}}$  both approaches yield identical results. In this regime, protein synthesis is the rate-limiting step. Indeed, on the time scale of gene expression the RNAP molecules have sufficient time to become well mixed in the cell. As a result, the effects of diffusion are negligible and the noise reduces to the expected value for a linear birth-and-death process.

However, for  $k_{\text{prod}} \gtrsim 1\text{s}^{-1}$ , spatial fluctuations can have a drastic effect on the noise in gene expression. In this regime, the noise of the spatially-resolved model is larger than that of the “well-stirred reactor” model. In fact, Fig. 5 shows that it grows fairly rapidly with increasing  $k_{\text{prod}}$ . The increase in noise is due to a very broad distribution of arrival times of RNAP molecules at the promoter site, much broader than the corresponding Poisson distribution for the system without spatial fluctuations. It is also seen that for very large production rates, the noise ultimately reaches a plateau value. At

these high values of  $k_{\text{prod}}$  the promoter site becomes an “absorbing” boundary for the RNAP molecules. Fig. 5 also reveals that the height of the plateau increases as the diffusion constant  $D$  becomes smaller. This is not surprising, because the importance of spatial fluctuations is expected to be larger for smaller diffusion constants. However, it does clearly show that in order to determine the significance of spatial fluctuations in gene expression, it is of interest to establish the value of the diffusion constant of the RNA polymerase experimentally.

Our model of gene expression is obviously highly simplified. Moreover, in our model, the increase in noise due to spatial fluctuations only occurs for protein synthesis rates that are unrealistically high, i.e. on timescales much faster than minutes as observed experimentally [13]. It remains yet to be seen how significant the effect of spatial fluctuations is on noise in gene expression.

### C. Gene expression II

The systems discussed above were radially symmetric: molecules  $B$  have to diffuse to the center of the container where they can react with molecule  $A$ . If we would have assumed that  $B$  molecules do not interact with each other, then we could have exploited the radial symmetry of the problem by using the radially symmetric Green’s functions [9].

Here we present a simple model of gene expression that is not radially symmetric. The reaction network is given

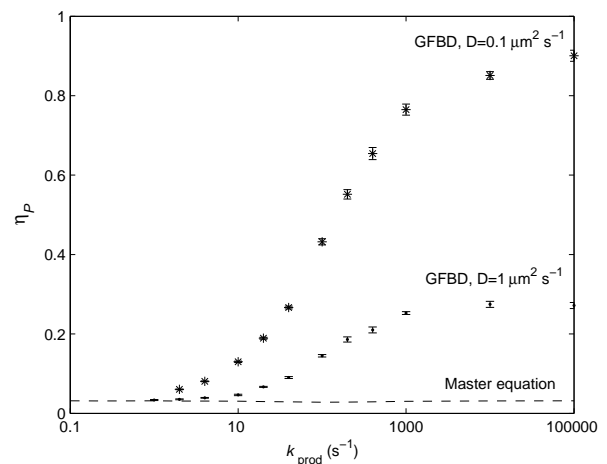
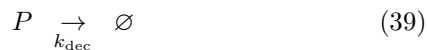
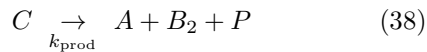


FIG. 5: The noise in protein level  $\eta_P$  as a function of protein production rate  $k_{\text{prod}}$  for the reaction scheme shown in Eqs. 30 – 32. Compared are the results obtained by GFBD with a diffusion constant of  $D = 1\mu\text{m}^2\text{s}^{-1}$  ( $\cdot$ ) and  $D = 0.1\mu\text{m}^2\text{s}^{-1}$  ( $*$ ) and the result using the chemical master equation (dashed line). The mean number of proteins was held constant at  $\bar{N}_P = 1000$  by changing the degradation rate  $k_{\text{decay}}$  of the protein.

by:



In this model,  $B$  is no longer a RNAP molecule, but a transcription factor that can dimerize to form the dimer  $B_2$ . This dimer can act as an activator: it can bind to the DNA and thereby recruit the RNAP to the promoter site [16]. Here, we do not model the RNAP explicitly. We will assume that when a dimer binds to the DNA, a RNA polymerase will also bind instantly to the promoter. Hence, if a dimer is bound to the DNA, gene expression will be induced with a probability  $k_{\text{prod}}/(k_d + k_{\text{prod}})$ . Here, we also point out that in the previous model we could have interpreted the  $B$  particles as transcription factors, rather than RNAP molecules. This is of interest, because it allows us to study the effect of cooperativity on the noise in gene expression.

In the simulations, we use the same setup as before with the promoter site ( $A$ ) in the center of a spherical container. The monomers can form dimers  $B_2$  with the same rate constants  $k_a$  and  $k_d$  as used in the model in the previous section. The dimerization reaction can occur anywhere in the container. The dimers can diffuse towards the center of the box to bind to the promoter, again with forward rate  $k_a$  and backward rate  $k_d$ .

In order to test the scheme, we first study the above network *without* protein synthesis ( $k_{\text{prod}} = 0$ ). Fig. 6 shows the probability  $p_{\text{bound}}$  that a dimer  $B_2$  is bound to the promoter site, as a function of the number of  $B$  molecules. As the concentrations of the monomers and dimers are low, the spatial correlations are expected to be negligible. This means that it becomes useful to compare the simulation results to the mean-field prediction using the macroscopic rate equations. Fig. 6 shows that, indeed, we find excellent agreement between the numerical results and the mean-field prediction. For comparison, we have also shown the results of the model discussed in the previous section, in which the  $B$  particles bind as monomers, rather than dimers. It is seen that cooperative binding turns a hyperbolic response into a sigmoidal response – a well-known ‘recipe’ of nature to enhance the steepness of a response.

We now turn to the effect of cooperativity on the noise in gene expression. Fig. 7 shows the noise in protein number as a function of the production rate. As in the previous model with non-cooperative binding of the activator, we have tuned the decay rate such that the average number of proteins is fixed at  $\bar{N}_P = 1000$  – this allows for a direct comparison of the two models. Fig. 7 reveals that both models yield similar results in the limiting regimes of small and large production rate  $k_{\text{prod}}$ .

However, it also shows that the increase in noise due to spatial fluctuations sets in at lower production rates in the cooperative binding scenario as compared to the non-cooperative case. The reason is that, in the cooperative binding scenario, dimerization leads to a lower effective concentration of the active form of the transcription factor, which, in turn, leads to a larger distribution of arrival times to the promoter site.

#### D. Performance

The essence of the GFBD scheme is to exploit the analytical solution of the Smoluchowski equation for a pair of interacting particles to set up an event-driven algorithm. This allows GFBD to make large jumps in time when the particles are far apart from each other. Clearly, the performance of the algorithm depends on the density of the system: the further the particles are apart from each other, the larger the time step that can be used and the better GFBD will perform in comparison to brute-force Brownian Dynamics schemes (see section II A). It is thus of interest to compare the distribution of propagation times in GFBD to the time step used in a brute-force Brownian Dynamics scheme as a function of density.

In figure 8 we show the distribution of propagation times  $\Delta t$  for the bimolecular reaction described in section III A as a function of density. For  $N_B = 18$  ( $[B] = 30$  nM), the value used in the above models of gene expression, the distribution has a maximum at  $\Delta t = 1 \cdot 10^{-4}$  s. Note also that the propagation times become smaller if

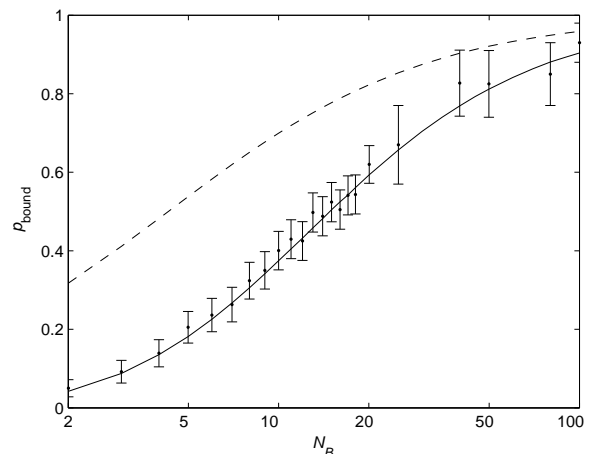


FIG. 6: The probability  $p_{\text{bound}}$  of finding a dimeric activator  $B_2$  bound to the promoter as a function of the total number of  $B$  particles for the reaction scheme shown in Eqs. 36 – 37 ( $k_{\text{prod}} = 0$ ); the volume of the container is  $V = 1\mu\text{m}^3$ . The GFBD results ( $\cdot$ ) are compared to the mean-field prediction as obtained by solving the macroscopic rate equations in 36 – 37 in steady-state (solid line). For comparison, we have also shown the mean-field prediction for the case without cooperative binding (dashed line).

the density increases. For  $[B] = 1\mu\text{M}$ , the peak in the distribution shifts to  $\Delta t = 1 \cdot 10^{-6}\text{s}$ .

In biochemical networks, concentrations are often very low. In gene networks, the concentrations of the gene regulatory proteins are often in the nM regime. Also in signal transduction networks the concentrations of the components are often fairly low, i.e. in the  $\mu\text{M}$  range. The analysis presented here, suggests that with GFBD it should be possible to reach time steps of at least  $10^{-6} - 10^{-4}\text{s}$ . In contrast, in a brute-force Brownian Dynamics simulation, we have to use a time step of at most  $10^{-10} - 10^{-9}\text{s}$  ( $10^{-3} - 10^{-2}\sigma^2/D$ ) in order to preserve the correct distribution (as, for instance, defined by the requirement that the analytical solution for the Green's function  $p(\mathbf{r}, t|\mathbf{r}_0, t_0)$  as shown in Fig. 2 can be reproduced). We thus believe that under biologically relevant conditions, GFBD can be three to six orders of magnitude faster than conventional schemes to simulate biochemical networks.

#### IV. CONCLUSIONS

We have developed a new technique, called Green's Function Brownian Dynamics, to simulate biochemical networks at the particle level and in both time and space. The main idea of the technique is to choose the time step such that only single particles or pairs of particles have to be considered. For these particles, the Smoluchowski equation can be solved analytically using Green's func-

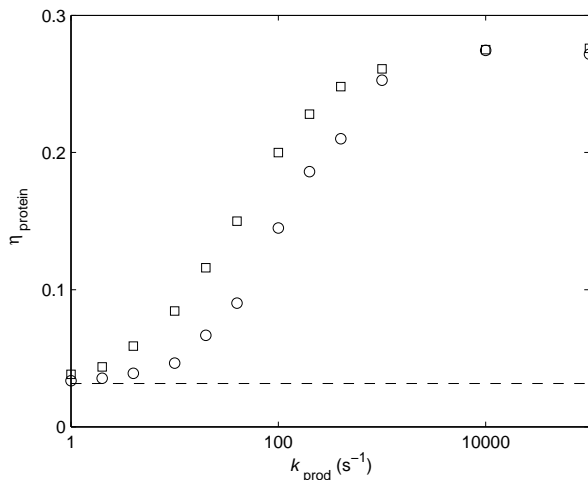


FIG. 7: The noise in protein concentration,  $\eta_p$ , as a function of the protein production rate for the reaction schemes shown in Eqs. 30 – 32 ( $\square$ ) and Eqs. 36 – 39 ( $\circ$ ). The former reaction scheme corresponds to non-cooperative binding of the activator, while the latter reaction scheme corresponds to cooperative binding of the activator. In both cases, the degradation rate  $k_{\text{decay}}$  of the protein was tuned such that the mean protein number is constant and equal to  $\overline{N}_P = 1000$ . The dashed line indicates the noise level  $\eta_p = 1/\sqrt{\overline{N}_P}$  of a corresponding linear birth-and-death process.

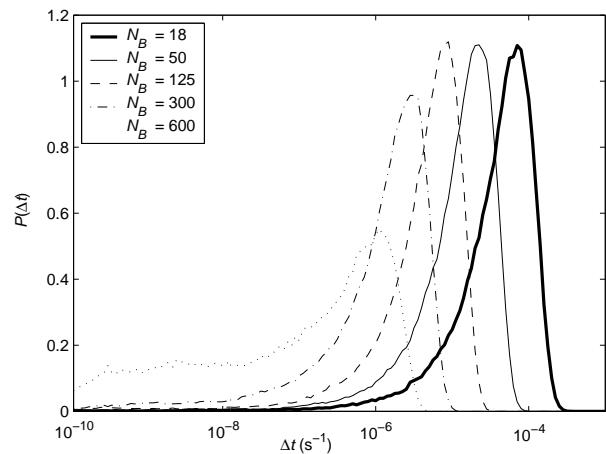


FIG. 8: The distribution of propagation times  $\Delta t$  for a system consisting of a single particle  $A$  in the center of a spherical box of volume  $V = 1\mu\text{m}^3$ , surrounded by  $N_B$  particles  $B$ ; the particles  $A$  and  $B$  can react according to a bimolecular reaction scheme (see Eq. 28). The distributions are shown for  $N_B = 18$  (bold solid line),  $N_B = 50$  (solid line),  $N_B = 125$  (dashed line),  $N_B = 300$  (dashed-dotted line) and  $N_B = 600$  (dotted line), corresponding to a concentration of  $[B] = 30$  nM,  $[B] = 83$  nM,  $[B] = 210$  nM,  $[B] = 500$  nM, and  $[B] = 1000$  nM, respectively. In the GFBD simulations, we use a lower cut-off for the propagation time,  $2.5 \cdot 10^{-10}\text{s}$ , which corresponds to the time step used in a brute-force Brownian Dynamics simulation.

tions. The analytical solution can then be used to set up an event-driven algorithm, quite analogous to the kinetic Monte Carlo schemes as originally developed by Bortz, Kalos and Elowitz [17] to simulate Ising spin systems and by Gillespie to numerically solve the chemical master equation [4, 5]. We would like to stress, however, that in contrast to the widely used ‘‘Gillespie’’ algorithm, our technique makes it possible to simulate biochemical networks at the particle level and in both time and space.

The analysis presented in section III D shows that GFBD is highly efficient. This should make it possible to simulate biochemical networks at much larger length and time scales than hitherto possible. Yet, we believe that the performance of the scheme can even be improved. In the current scheme, we use a global maximum time step that pertains to all particles in the system. It seems natural, however, to assign to each particle an individual maximum time step. In such a scheme, each particle would have its own individual clock. This approach would make it possible to devote all computational effort to those particles that interact frequently; the particles that initially are far apart from other particles are only updated after the time has come that they have a reasonable chance to interact. A second possible improvement would be to exploit the low concentration of the components in another way. In the current scheme, we explicitly take into account excluded volume interactions. In fact, this often poses a limit on the maximum time step. If

the concentrations are low, however, we should expect that the excluded volume effects are negligible for the behaviour of the network. In future work, we will show that these observations can be incorporated into the algorithm to enhance the performance of Green's Function Brownian Dynamics even further.

### Acknowledgements

We would like to thank Daan Frenkel for useful discussions and suggestions. The work is part of the research

program of the ‘‘Stichting voor Fundamenteel Onderzoek der Materie (FOM)’’, which is financially supported by the ‘‘Nederlandse organisatie voor Wetenschappelijk Onderzoek (NWO)’’.

### Appendix A: Solution of Smoluchowski equation

The Green's function  $p(\mathbf{r}, t | \mathbf{r}_0, t_0)$  for a pair of particles  $A$  and  $B$ , initially separated by a distance  $r_0$ , that move by free diffusion, but, upon contact can react with a rate constant  $k_a$ , is derived in [9]. It is given by

$$p(r, \theta, \phi, t | r_0) = \frac{1}{4\pi\sqrt{rr_0}} \sum_{n=0}^{\infty} (2n+1) P_n(\cos\theta) \int_0^{\infty} e^{-Du^2t} F_{n+1/2}(ur) F_{n+1/2}(ur_0) u du, \quad (40)$$

where

$$F_\nu(ur) = \frac{(2\sigma k_a + 1)[J_\nu(ur)Y_\nu(u\sigma) - Y_\nu(ur)J_\nu(u\sigma)] - 2u\sigma[J_\nu(ur)Y'_\nu(u\sigma) - Y_\nu(ur)J'_\nu(u\sigma)]}{[(2\sigma k_a + 1)J_\nu(u\sigma) - 2u\sigma J'_\nu(u\sigma)]^2 + [(2\sigma k_a + 1)Y_\nu(u\sigma) - 2u\sigma Y'_\nu(u\sigma)]^2}^{1/2}, \quad (41)$$

and where  $P_n$  is the  $n$ th Legendre polynomial,  $J_n$  and  $Y_n$  are the  $n$ th Bessel function of the first and the second kind,  $D = D_A + D_B$  is the total diffusion constant of the two particles  $A$  and  $B$  and  $\sigma$  is the particle diameter. The Green's function can be expressed in a more compact notation by

$$p(r, \theta, \phi, t | r_0) = \sum_{n=0}^{\infty} C_n P_n(\cos\theta) R_n(r, t). \quad (42)$$

The probability  $f(r | r_0, t)$  of finding the particles separated by a distance between  $(r, r + dr)$  at time  $t$  is given by

$$f(r | r_0, t) = 2\pi \sum_{n=0}^{\infty} C_n Q_n(\pi) r^2 R_n(r, t), \quad (43)$$

with

$$Q_n(\theta) = \int_0^\theta \sin\theta P_n(\cos\theta) d\theta. \quad (44)$$

The conditional probability  $g(\theta | r, r_0, t)$  that two particles are at an angle between  $(\theta, \theta + d\theta)$  with respect to the original direction  $\mathbf{r}_0 = \mathbf{r}_B - \mathbf{r}_A$ , given that they are separated by a distance  $r$  at time  $t$ , is

$$g(\theta | r, r_0, t) = 2\pi \sum_{n=0}^{\infty} C_n Q'_n(\theta) r^2 R_n(r, t). \quad (45)$$

The survival probability  $S(t)$  is given by

$$S(t) = \int_\sigma^\infty f(r | r_0, t) dr. \quad (46)$$

The above integral is complicated but it follows from the properties of the diffusion equation that it must be identical to the familiar survival probability for the spherically symmetric case [8, 15].

The above distribution functions suggest a straightforward procedure for drawing a new position  $\mathbf{r}$  from the Green's function  $p(\mathbf{r}, t | r_0)$ . We pre-tabulate  $Q_n(\theta)$  and  $R_n(r, r_0, t)$  up to a certain order  $N$ . From this we construct the probability distribution  $f(r | r_0, t)$  and we draw a new distance  $r$  from this distribution. Next, we draw  $\theta$  from the distribution  $g(\theta | r, r_0, t)$  and finally we chose  $\phi$  uniformly distributed between 0 and  $2\pi$ .

This procedure works well for large  $t$ . For small  $t$ , however, the above procedure becomes rather cumbersome as the number of terms  $N$  that needs to be included in order for the summations in Eqs. 43 and 45 to converge, becomes very large. The reason is that  $p(\mathbf{r}, t | r_0)$  becomes a sharply peaked function around  $\mathbf{r}_0$  for small  $t$ . However, for small  $t$ , the probability that the two particles will interact with each other, is relatively small. In other words, for small  $t$  the full solution  $p(\mathbf{r}, t | r_0)$ , is dominated by free diffusion. We can exploit this observation in order to reduce  $N$  by writing the Greens's function as  $p(\mathbf{r}, t | r_0) = p_{\text{free}}(\mathbf{r}, t | r_0) + p_{\text{corr}}(\mathbf{r}, t | r_0)$ , where  $p_{\text{free}}$  is the solution for free diffusion and  $p_{\text{corr}}$  is a correction term that takes into account the reacting boundary at  $r = \sigma$ . As the correction term  $p_{\text{corr}}$  is usually rather small for small  $t$ , the number of terms  $N$  that needs to be included in order for the summations in Eqs. 43 and 45 to converge, is strongly reduced.

Using the fact, that  $p_{\text{free}}$  can be expanded as

$$p_{\text{free}}(r, \theta, \phi, t|r_0) = \frac{1}{4\pi\sqrt{rr_0}} \sum_{n=0}^{\infty} (2n+1)P_n(\cos\theta) \int_0^{\infty} e^{-Du^2t} J_{n+1/2}(ur)J_{n+1/2}(ur_0)udu, \quad (47)$$

we find that  $p_{\text{corr}}$  can be expressed as

$$p_{\text{corr}}(r, \theta, \phi, t|r_0) = \frac{1}{4\pi\sqrt{rr_0}} \sum_{n=0}^{\infty} (2n+1)P_n(\cos\theta) \int_0^{\infty} e^{-Du^2t} \frac{R_1}{R_1^2 + R_2^2} (R_1F_1 + R_2F_2)udu, \quad (48)$$

where

$$R_1 = (2\sigma k_a + 1)J_{n+\frac{1}{2}}(u\sigma) - 2u\sigma J'_{n+\frac{1}{2}}(u\sigma), \quad (49)$$

$$R_2 = (2\sigma k_a + 1)Y_{n+\frac{1}{2}}(u\sigma) - 2u\sigma Y'_{n+\frac{1}{2}}(u\sigma), \quad (50)$$

$$F_1 = J_{n+\frac{1}{2}}(ur)J_{n+\frac{1}{2}}(ur_0) - Y_{n+\frac{1}{2}}(ur)Y_{n+\frac{1}{2}}(ur_0), \quad (51)$$

$$F_2 = J_{n+\frac{1}{2}}(ur)Y_{n+\frac{1}{2}}(ur_0) + J_{n+\frac{1}{2}}(ur_0)Y_{n+\frac{1}{2}}(ur). \quad (52)$$

### Appendix B: Proof of the algorithm

Let  $P(t, \mu)dt$  be the probability that the next reaction will occur in the time interval between  $t$  and  $t + dt$  and will be reaction  $R_\mu$ . As described in section II B, the time step is chosen such that the reactions occur *independently* from each another. The probability  $P(t, \mu)dt$  is therefore given by

$$P(t, \mu)dt = q_\mu(t)dt \prod_{\substack{\nu=1 \\ \nu \neq \mu}}^M S_\nu(t). \quad (53)$$

As mentioned in section II E, the algorithm features a maximum time step. It is thus conceivable that not a single reaction occurs within a time step. The probability  $Q(\Delta t_{\text{max}})$  that no reaction occurs within a time step of size  $\Delta t_{\text{max}}$  is given by

$$Q(\Delta t_{\text{max}}) = \prod_{\nu=1}^M S_\nu(\Delta t_{\text{max}}). \quad (54)$$

It can easily be shown that the procedure outlined section II E is consistent with Eqs. 53 and 54. Let  $\tilde{Q}(\Delta t_{\text{max}})$  be the probability that the procedure described above does not yield a reaction within the time step of size  $\Delta t_{\text{max}}$ . It is given by

$$\tilde{Q}(\Delta t_{\text{max}}) = \text{Prob}(t_\nu > \Delta t_{\text{max}} \text{ for all } \nu) \quad (55)$$

$$= \prod_{\nu=1}^M \xi_\nu > (1 - S_\nu(\Delta t_{\text{max}})) \quad (56)$$

$$= \prod_{\nu=1}^M S_\nu(\Delta t_{\text{max}}) \quad (57)$$

$$= Q(\Delta t_{\text{max}}). \quad (58)$$

Similarly, let  $\check{P}(t, \mu)dt$  be the probability that the above described procedure yields, at time  $t$ , reaction  $R_\mu$  as the next reaction. It is given by

$$\check{P}(t, \mu)dt = \text{Prob}(t < t_\mu < t + dt) \times \text{Prob}(t_\nu > t_\mu \text{ for all } \nu \neq \mu) \quad (59)$$

$$= q_\mu(t)dt \prod_{\substack{\nu=1 \\ \nu \neq \mu}}^M \text{Prob}(\xi_\nu > (1 - S_\nu(t_\nu))) \quad (60)$$

$$= q_\mu(t)dt \prod_{\substack{\nu=1 \\ \nu \neq \mu}}^M S_\nu(t_\nu) \quad (61)$$

$$= P(t, \mu)dt. \quad (62)$$

- 
- [1] N. G. van Kampen, *Stochastic Processes in Physics and Chemistry*, North-Holland, Amsterdam (1992).  
[2] Y. Togashi and K. Kaneko, Phys. Rev. Lett **86**, 2459 (2001).  
[3] N. M. Shnerb, Y. Louzoun, E. Bettelheim and S. Solomon, Proc. Natl. Acad. Sci. **97**, 10322 (2000).  
[4] D. T. Gillespie, J. Comput. Phys. **22**, 403 (1976).  
[5] D. T. Gillespie, J. Phys. Chem. **81**, 2340 (1977).  
[6] C. J. Morton-Firth and D. Bray, J. Theor. Biol. **192**, 117 (1998).  
[7] B. Alberts, D. Bray, J. Lewis, M. Raff, J. Lewis, M. Raff, K. Roberts, and J. D. Watson, *Molecular Biology of the Cell*, Garland Publishing, New York, (1994).  
[8] H. Kim and K. J. Shin, Phys. Rev. Lett. **82**, 1578 (1999).  
[9] H. S. Carslaw and J. C. Jaeger, *Conduction of Heat in Solids*, Oxford University Press, New York(1959).  
[10] N. Agmon, A. Szabo, J. Chem. Phys. **92**, 5270 (1990).  
[11] J.-P. Hansen & I. R. McDonald, *Theory of simple liquids*, 2nd edn, Academic Press, San Diego (1986).  
[12] M. B. Elowitz, M. G. Surette, P.-E. Wolf, J. B. Stock, and S. Leibler, J. Bacteriol. **181**, 197 (1999).  
[13] P. S. Swain, M. B. Elowitz and E. D. Siggia, Proc. Natl. Acad. Sci. **99**, 12795 (2002).  
[14] H. X. Zhou and A. Szabo, J. Chem. Phys. **95**, 5948 (1991).  
[15] S. A. Rice, *Diffusion Limited Reactions*, Elsevier Science

- Publishing, New York (1985).
- [16] M. Ptashne & A. Gann *Genes and signals*. Cold Spring Harbor Laboratory Press, New York (2002).
- [17] , A. B. Bortz, M. H. Kalos, and J. L. Lebowitz, *J. Comp. Phys.* **17**, 10 (1975).